

# Causal Structure Representation Learning of Confounders in Latent Space for Recommendation

Hangtong Xu  
MIC Lab, College of Computer  
Science and Technology, Jilin  
University  
Changchun, China  
xuht21@mails.jlu.edu.cn

Yuanbo Xu\*  
MIC Lab, College of Computer  
Science and Technology, Jilin  
University  
Changchun, China  
yuanbox@jlu.edu.cn

Yongjian Yang  
MIC Lab, College of Computer  
Science and Technology, Jilin  
University  
Changchun, China  
yyj@jlu.edu.cn

## ABSTRACT

Inferring user preferences from the historical feedback of users is a valuable problem in recommender systems. Conventional approaches often rely on the assumption that user preferences in the feedback data are equivalent to the real user preferences without additional noise, which simplifies the problem modeling. However, there are various confounders during user-item interactions, such as weather and even the recommendation system itself. Therefore, neglecting the influence of confounders will result in inaccurate user preferences and suboptimal performance of the model. Furthermore, the unobservability of confounders poses a challenge in further addressing the problem. To address these issues, we refine the problem and propose a more rational solution. Specifically, we consider the influence of confounders, disentangle them from user preferences in the latent space, and employ causal graphs to model their interdependencies without specific labels. By cleverly combining local and global causal graphs, we capture the user-specificity of confounders on user preferences. We theoretically demonstrate the identifiability of the obtained causal graph. Finally, we propose our model based on Variational Autoencoders, named Causal Structure representation learning of Confounders in latent space (CSC). We conducted extensive experiments on one synthetic dataset and five real-world datasets, demonstrating the superiority of our model. Furthermore, we demonstrate that the learned causal representations of confounders are controllable, potentially offering users fine-grained control over the objectives of their recommendation lists with the learned causal graphs.

## CCS CONCEPTS

• **Information systems** → **Recommender systems.**

## KEYWORDS

Causal structure, Preference modeling, Confounders, Variational inference

\*Corresponding Author: Yuanbo Xu

Permission to make digital or hard copies of all or part of this work for personal or classroom use is granted without fee provided that copies are not made or distributed for profit or commercial advantage and that copies bear this notice and the full citation on the first page. Copyrights for components of this work owned by others than ACM must be honored. Abstracting with credit is permitted. To copy otherwise, or republish, to post on servers or to redistribute to lists, requires prior specific permission and/or a fee. Request permissions from [permissions@acm.org](https://permissions.acm.org).

Conference acronym 'XX, June 03–05, 2018, Woodstock, NY

© 2018 Association for Computing Machinery.  
ACM ISBN 978-1-4503-XXXX-X/18/06...\$15.00  
<https://doi.org/XXXXXXX.XXXXXXX>

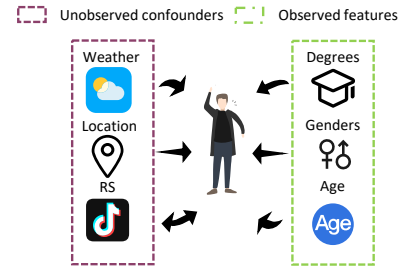


**Figure 1: An example illustrating that user preferences in the feedback data are influenced by both the users themselves and external confounders.**

## ACM Reference Format:

Hangtong Xu, Yuanbo Xu, and Yongjian Yang. 2018. Causal Structure Representation Learning of Confounders in Latent Space for Recommendation. In *Proceedings of Make sure to enter the correct conference title from your rights confirmation email (Conference acronym 'XX)*. ACM, New York, NY, USA, 10 pages. <https://doi.org/XXXXXXX.XXXXXXX>

## 1 INTRODUCTION

Recommender systems play a vital role in information technology, aiming to assist users in discovering content or products that might align with their interests. User historical feedback data is a crucial basis for model prediction of user preferences. Based on this, many highly effective methods have been proposed, such as MultiVAE [5], MacridVAE [15], etc. Existing work often assumes that user preferences in historical feedback data are noise-free, focusing on fitting the feedback data to achieve good model performance.

However, various confounders inevitably influence users during the interaction process, affecting their final decisions. As shown in Figure 1, user preferences are influenced by both the intrinsic characteristics of users (e.g., gender, age) and external confounders in the interaction environment (e.g., weather, location). For example, when analyzing user reviews for a specific product like ice cream in an online retail platform, we observe varying preferences among users due to confounders – some users may exhibit opposite feedback regarding their preferences for ice cream. For instance, the weather at the time of purchase is a confounder. On hot days, users tend to give more positive feedback for ice cream due to its refreshing nature, even if it's not their favorite flavor. On the other hand, during colder seasons, the same users might give less favorable feedback. Thus, it's evident that user preferences, as reflected

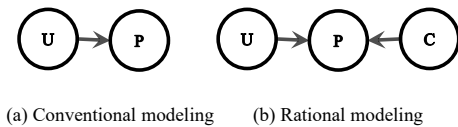


**Figure 2: Conventional modeling versus a more rational modeling approach. Left is the conventional modeling and right is the rational modeling proposed in this work.**

in the feedback data, are a combination of the intrinsic characteristics of users and external confounders like weather, representing the interplay of both intrinsic and extrinsic influences. This also explains why models improve performance when additional information such as time and location, is incorporated. Unfortunately, most confounders are unobservable, and we cannot obtain corresponding labels from users as additional information. Hence, we cannot explicitly model confounders to separate them from user preferences.

To address these challenges, we first reformulate the user preference prediction problem by introducing the influence of confounders. In this way, user preferences in the feedback data stem from the combined impact of the inherent preferences of users and external confounders. We proposed a mild assumption of confounder independence to disentangle confounders from user preferences in the latent space. Specifically, we assumed that the influence of all confounders on each user originates from the same set of confounders, which ensures user independence of confounders. Furthermore, we found that confounders are not independent of each other. For example, the weather depends on users' location. We utilized a causal structural model (SEM) to represent the generation process of confounders. Specifically, we employed a binary matrix to denote the global causal graph, where directed edges signify the dependency relationships between confounders. However, for different users, the relationships between confounders also vary, sometimes being opposite. Thus, we used an additional local causal graph to capture the user-specificity of confounders. Furthermore, we demonstrate that the learned causal representations of confounders are controllable, potentially offering users fine-grained control over the objectives of their recommendation lists with the learned causal graphs. Finally, we combine the obtained causal representations of confounders with the inherent preferences of users to fit user preferences in historical feedback data, proposed a model based on Variational Autoencoder (VAE) named Causal Structure representation learning of Confounders in latent space (CSC) to learn causal representations of user preferences and confounders simultaneously. In addition, we theoretically proved the identifiability of the model.

The contributions of our work can be summarized as follows: (1) We have re-formalized the problem of user preference prediction, providing a more reasonable modeling approach for user preferences. (2) We introduced a mild assumption that allows for the independent representation of user preferences and the influence of confounders and utilized causal graphs to capture the dependencies among confounders. Furthermore, we provide the proof of the identifiability of the causal graph. (3) We employed

global and local causal graphs to capture the invariance and specificity between users and confounders. We proposed a model based on the Variational Autoencoder (VAE) to learn causal representations of user preferences and confounders simultaneously. (4) We conducted extensive experiments on a synthetic dataset and five real-world datasets to demonstrate the effectiveness of our model. (5) We demonstrate that the learned causal representations of confounders are controllable, potentially offering users fine-grained control over the objectives of their recommendation lists with the learned causal graphs. Our code is publicly available at: <https://anonymous.4open.science/r/CSC><sup>1</sup>.

## 2 METHODOLOGY

This section thoroughly introduces our proposed model with the necessary theoretical proofs.

### 2.1 A More Rational Architecture

Predicting user preferences from their historical interaction data is a common training paradigm in the domain of recommender systems and is generally based on the fundamental assumption that the user preferences contained in the feedback data reflect the true preferences of the user. Based on such assumptions, the user preference prediction problem can be formulated as follows:

**PROBLEM 1.** Given the historical interaction data  $x_u = \{x_{u,1}, \dots, x_{u,n}\}$ <sup>2</sup>, we can predict the user preference  $z_u$  with the model parameter  $\phi$ .

$$q_\phi(z_u|x_u).$$

As Figure 2 (a) shows, The fundamental assumption of the problem is that the users themselves solely influence the user preferences in the data. Numerous outstanding approaches have arisen to address the above problem, and their solutions can be uniformly summarised into one class of solutions, i.e., for a user, they assume the observed data is generated from the following distributions:

$$p_\theta(x_u) = E \left[ \int p_\theta(x_u|z_u)p_\theta(z_u)dz_u \right]. \quad (1)$$

Such approaches will restore the generation process of the data with outstanding performance, but they overlook the influence of confounders on feedback in user interactions. As a result, they cannot explain why the user feedback on ice cream shows opposite results due to weather, where weather acts as a confounder. Based on the above findings, we naturally consider incorporating confounders into the data generation process as a more reasonable modeling approach. Firstly, we redefine the problem as follows:

**PROBLEM 2.** Given the historical interaction data  $x_u = \{x_{u,1}, \dots, x_{u,n}\}$ , we can predict the user preference  $z_u, c_u$  with the model parameter  $\phi$ .

$$q_\phi(z_u, c_u|x_u).$$

A graphical representation is depicted in Figure 2 (b), illustrating that the inner preferences of users and other confounders influence the observed user preferences in feedback data. We must emphasize that we are exclusively considering unobserved confounders in this problem. For observable confounders, we prefer incorporating them as additional input to enhance the performance of models. In

<sup>1</sup>Our code will be made public as soon as it is organized and ready.

<sup>2</sup> $x_{u,i} \in \{0, 1\}$ ,  $x_{u,i} = 1$  representing an interaction between user  $u$  and item  $i$ .

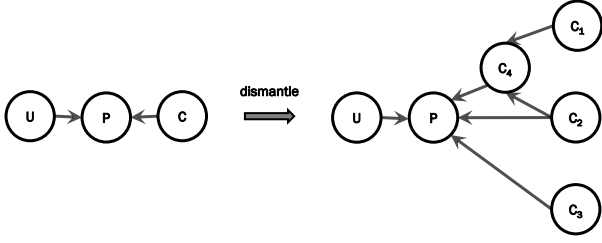


**Figure 3: An example showing disentanglement in latent space, where the confounders are further dismantled based on the given causal graph.**

a similar vein, we propose a feasible solution to the aforementioned problem as follows:

$$p_{\theta}(x_u) = E_{p_{\theta}(c_u)} \left[ \int p_{\theta}(x_u | z_u, c_u) p_{\theta}(z_u) dz_u \right]. \quad (2)$$

By employing this approach, we can effectively disentangle user preferences from confounders, thus overcoming the limitations of conventional methods. For example, we can use the do-operation to predict user interactions in their current environment, enabling us to answer a counterfactual question such as "Will users prefer ice cream if the weather is warm?". Even when the labels of the relevant confounders are unknown, we can obtain purer representations of users' preferences than composite entities.

## 2.2 Causal Modeling of Unobserved Confounders

When users interact with items, they are inevitably influenced by confounders such as weather, location, etc. Hence, many models that utilize additional information such as location data as supplementary input often demonstrate better predictive performance. However, observable confounders represent only a small fraction of this vast population. In most cases, confounders are unobservable. Therefore, disentangling the impact of unobservable confounders from feedback data remains challenging. To address this issue, we start by making a mild assumption on the independence of the confounders:

**ASSUMPTION 1.** *Given confounders  $C = \{c_1, c_2, \dots, c_k\}$ , we assume that is independent of the user.*

$$c_j \perp u_i, \quad i \in [1, m], j \in [1, k].$$

One premise for this assumption is that the data collection environment for user feedback is consistent. This condition is often easily met in recommender systems, where data is sourced from historical interactions within a specific platform over a certain period. Hence, this assumption is reasonably mild and applies to most recommendation scenarios. With this assumption, we can separate the confounders from the inherent preferences of users, thus achieving the model architecture as depicted in Eq 2.

However, the relationships among confounders are not independent and follow a causal structure represented by a specific causal graph. For instance, consider two confounders: weather and location. As illustrated in Figure 1, the weather during user interaction

depends on users' location. To formalize the causal representation, we consider  $k$  confounders in the data. The confounders are causally structured by a Directed Acyclic Graph (DAG) with an adjacency matrix  $A$ . For convenience, we adopt a linear Structural Causal Model (SCM) to model the relationship between confounders and the causal graph, as illustrated in Eq 3:

$$C = A^T C + \epsilon = (I - A^T)^{-1} \epsilon, \quad (3)$$

where  $A$  is the parameter to be learned by our model,  $\epsilon$  is independent Gaussian noise, and  $C$  is a structured causal representation of the  $n$  confounders generated by a DAG. This approach can further disentangle the confounders based on the causal graph  $A$ , as depicted in Figure 3. As expected, nonlinear SCM is more suitable for complex scenarios like recommender systems than linear ones. Therefore, in our practical deployment, we utilize the nonlinear SCM, which will be further elucidated in Section 2.3.

## 2.3 Causal Structure Learning

As discussed earlier, an accurate causal graph enables us to capture better the influence of confounders on user preferences and the dependencies among these confounders. In conventional causal graphs, a causal flow between nodes is typically represented by an adjacency matrix, and the weights in this matrix measure the influence of parent nodes on their respective child nodes, when applied in recommendation system scenarios, falls short in capturing the heterogeneity among users.

For example, consider two different users within the context of music recommendation. One user enjoys listening to different types of songs in various locations (e.g., listening to quiet music in a library), while the other user consistently prefers the same type of music regardless of the location. The impact of location on the two users is different—the location influences the former, while the latter is unaffected by it. Therefore, it is unreasonable to use the same causal graph to predict the effect of location on the music preferences of these two users. To address this issue, we employ a combination of global and local causal graphs to capture confounders' influence on user preferences.

**2.3.1 Global SCM.** Specifically, we use the global causal graph to model the relationships among all confounders. Given the adjacency matrix  $A$ , it is associated with the true causal graph. In this context,  $A_{ij}$  can be viewed as an indicator vector, where  $A_{ij} = 1$  signifies that node  $i$  is the parent node of node  $j$ , indicating that node  $j$  is influenced by node  $i$ . In contrast,  $A_{ij} = 0$  implies that node  $j$  and node  $i$  are unrelated. The global causal graph is primarily used to capture dependencies among confounders without focusing on the strength of the dependencies between any two dependent confounders.

Therefore, we only require a binary adjacency matrix to meet this need. To make the binary operation continuous, we leverage the *Gumbel-Softmax* to get the binary adjacency matrix, which gives a continuous approximation to sampling from the categorical distribution [7, 8, 15]. We adopt a similar approach by adding Gumbel noise in the sigmoid function, which we formula as *Gumbel-Sigmoid*:

$$\text{Gumbel-Sigmoid}(A) = \frac{\exp((A + \hat{g})/\tau)}{\exp((A + \hat{g})/\tau) + \exp(\hat{g}/\tau)}, \quad (4)$$

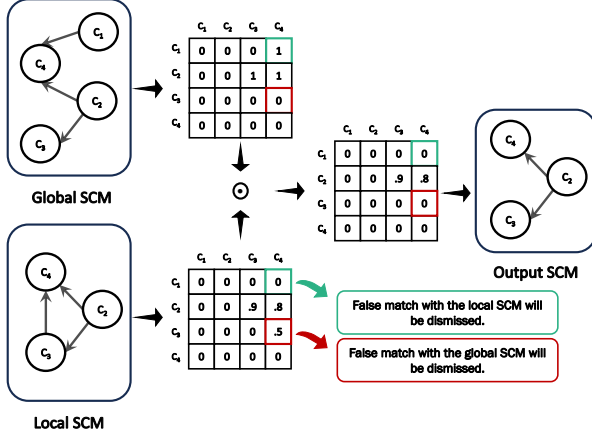


Figure 4: Example of a Global and Local Causal Structure.

where  $\dot{g}$  and  $\check{g}$  are two independent Gumbel noises, and  $\tau \in (0, \infty)$  is a temperature parameter. As  $\tau$  diminishes to zero, a sample from the *Gumbel-Sigmoid* distribution becomes cold and resembles the one-hot samples. Our experiments show that a small fixed  $\tau$  (e.g., 0.2) works well.

**2.3.2 Local SCM.** Once we obtain a global causal graph, we use local causal graphs to measure the strength of dependencies between confounders. In our model, the embeddings representing confounders are shared among users. Therefore, to capture user specificity, we must introduce additional user-specific information to distinguish between users. The conventional approach involves using additional user embeddings as personalized user information. However, this leads to increased computational complexity and parameters in the model. To mitigate this drawback, we utilize a linear layer to map the encoder output to obtain personalized user information without significantly increasing the temporal and spatial complexity of the model.

$$\mathbf{u} = \text{MLP}(z). \quad (5)$$

Where  $z$  is the output of the encoder, and  $u$  is the user-specific information after MLP Layer, as Figure 5 shows. By incorporating additional user-specific information, we can obtain distinct representations of confounders for each user. Furthermore, we utilize an attention mechanism to calculate the strength of dependencies between confounders. In our experiments, we observed that the multi-head attention performs better as it effectively captures the heterogeneity among different confounders.

$$W^{\text{local}} = \text{MultiHead}(\mathbf{C}, \mathbf{u}). \quad (6)$$

where the number of attention heads corresponds to the number of confounders. The attention layer is illustrated in Figure 5.

**2.3.3 Causal Layer.** Given the global causal graph and local causal graphs, we perform calculations in the causal layer to obtain the final user-specific causal graph.

$$A^u = \mathbf{A} \odot W^{\text{local}}. \quad (7)$$

where  $\odot$  is the element-wise multiplication. As Figure 4 shows,  $A_{ij}^u = 1$  if and only if both  $A_{ij} = 1$  and  $W_{ij}^{\text{local}} \neq 0$  hold, which reveals two reasonable potential conditions. Firstly, the local causal graphs must adhere to the global causal graph, meaning that in the global causal graph, any two confounders without a causal relationship cannot establish causality through the local causal graphs. The global causal graph is associated with the true causal graph. Therefore, any causal relationship absent in the global causal graph, even if it exists in the local causal graphs, is considered erroneous and not considered. Secondly, any two confounders without a causal relationship in the local causal graphs cannot influence the current user through the global causal graph. The local causal graphs capture the influence of confounders on the user. If there is no causal relationship between two confounders in the local causal graph, it implies that this causal pathway cannot influence the user. Hence, it is not considered as including such pathways would affect the final performance. Once we obtain the final causal graph, we can derive causal representations of the confounders according to Eq 3:

$$c_i = g_i(A_i^u \odot \mathbf{C}) + \epsilon_i, \quad (8)$$

where  $g_i(\cdot)$  is a mild nonlinear function. For any confounder  $c_i$ ,  $A_i^u \odot \mathbf{C}$  represents considering only the influence of its parent nodes, excluding the influence of other irrelevant nodes. Furthermore, this layer can also implement the "do-operation", we only need to provide an additional mask  $A^{\text{mask}}$ , where  $A_{ij}^{\text{mask}} = 0$  indicates excluding the influence of node  $i$  on node  $j$  in the do-operation.

**2.3.4 Identification of the Learned Graph.** As shown in Figure 5, we will utilize a parametric model like Variational Autoencoder (VAE), combined with a  $k \times k$  binary adjacency matrix, to fit the observed data. Unsupervised learning of the model might be infeasible due to the identifiability issue as discussed in [6, 10, 20]. To demonstrate the identifiability of the learned graph, we prove that under appropriate conditions, the computation described above can lead to the recognition of the hypergraph of the true graph. Consider a marginal distribution  $P(\mathbf{C})$  induced by a Structural Equation Model (SEM) defined in Eq 3 with Directed Acyclic Graph (DAG)  $\mathcal{G}$ , and our SEM Eq 8 induces the same marginal distribution, where the binary adjacency matrix represents a DAG  $\mathcal{H}$ , we can obtain Lemma 1 if the  $g_i(\cdot)$  is not a constant function and its proof is given in Appendix A.1.

**LAMMA 1.**  $\mathcal{H}$  is a super-graph of  $\mathcal{G}$ , i.e., all the edges in  $\mathcal{G}$  also exist in  $\mathcal{H}$ .

As [9][Theorem 27] shows, if the  $P(\mathbf{C})$  is generated by a restricted additive noise model (ANM), the true causal graph is identifiable. Thus, we further assume a restricted ANM for the data-generating procedure to ensure the true causal graph  $\mathcal{G}$  is identifiable. We then obtain the following proposition, with proof in Appendix A.2.

**PROPOSITION 1.** Assume a restricted ANM with graph  $\mathcal{G}$  and distribution  $P(\mathbf{C})$  so that the original SEM is identifiable. If the parameterized SEM in the form of Eq. 8 with graph  $\mathcal{H}$  induces the same  $P(\mathbf{C})$ , then  $\mathcal{H}$  is a super-graph of  $\mathcal{G}$ .

Then we can apply a parametric model and a binary adjacency matrix to fit the SEM in Eq. 8. If the causal relationships fall into

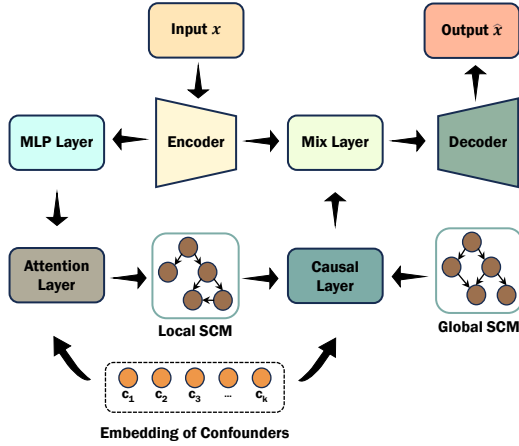


Figure 5: The CSC architecture.

the chosen model functions and we can obtain the exact solution that minimizes the negative log-likelihood given infinite samples, the resulting SEM has the same distribution [4]. Consequently, we obtain an acyclic supergraph from which existing nonlinear variable selection methods can be used to learn the parental sets and the causal graph.

## 2.4 Learning Strategy

The overall architecture of our model is depicted in Figure 5. This section describes how to train our model to simultaneously learn user causal preferences and graphs.

**2.4.1 Mix Layer.** The Mix layer combines the output of encoder  $z$  with the output of the causal layer - the causal representations of confounders, resulting in a user representation under the influence of confounders. This user representation is then input into the decoder to reconstruct observed data. Specifically, given  $z$  and  $c_i$ , we can obtain the user latent representation  $z_u$  under the influence of confounder  $i$ :

$$z_{u,i} = f(z_u, c_i), \quad (9)$$

where  $f(\cdot)$  is a non-linear function. For  $K$  confounders, a user may be influenced by some rather than all. To retain this characteristic, we initially measure the strength of influence using the cosine similarity function. Subsequently, we obtain a more skewed distribution using the *Gumbel-Sigmoid* in Eq 4 with  $\tau = 0.1$ .

$$\begin{aligned} s_k &= \text{Cosine-Similarity}(z, z_{u,k}), \\ w_k^c &= \text{Gumbel-Sigmoid}([s_1, \dots, s_k]). \end{aligned} \quad (10)$$

**2.4.2 Evidence Lower Bound.** Once we obtain the latent representation  $z_u$  of users, we can reconstruct the observed data as follows:

$$p_\theta(x_u|z_u, \mathbf{C}) = \sum_{k=1}^K w_k^c \cdot g_\theta(z_{u,k}). \quad (11)$$

We follow the variational autoencoder (VAE) paradigm [2] and optimize  $\theta$  by maximizing the lower bound  $\sum_u \ln p_\theta(x_u)$ , where

Dataset	#Interactions	#User	#Items	#Sparsity
ML-100k	100,000	943	1,682	93.69%
ML-1M	1,000,209	6,040	3,706	95.54%
ML-20M	20,000,263	138,493	26,744	99.46%
Yelp	2,672,630	96,170	160,031	98.79%
TaFeng	687,410	202,56	23,534	99.96%

Table 1: Statistics of the datasets

$\ln p_\theta(x_u)$  is bounded as follows:

$$\begin{aligned} \ln p_\theta(x_u) &\geq E_{p_\theta(\mathbf{C})} \{ E_{q_\theta(z_u|x_u, \mathbf{C})} [\ln p_\theta(x_u|z_u, \mathbf{C})] \\ &\quad - D_{KL}(q_\theta(z_u|x_u, \mathbf{C}) \| p_\theta(z_u)) \} . \end{aligned} \quad (12)$$

The relevant proofs are provided in Appendix A.3.

**2.4.3 Constraints of the Causal Graph.** The causal adjacency matrix  $\mathbf{A}$  is constrained to be a DAG. We employ a continuous distinguishable constraint function instead of the traditional combinatorial DAG constraint. This function attains 0 if, and only if the adjacency matrix  $\mathbf{A}$  corresponds to a DAG [21].

$$\mathbf{H}(\mathbf{A}) = \text{tr}((\mathbf{I} + \frac{c}{k} \mathbf{A} \odot \mathbf{A})^k) - k = 0, \quad (13)$$

where  $c$  is an arbitrary positive number, and  $k$  is the number of confounders. The value of  $c$  is the spectral radius of  $\mathbf{B}$ , and due to nonnegativity, it is bounded by the maximum row sum by the Perron-Frobenius theorem.

**2.4.4 Objective function.** The training procedure of our model reduces to the following constrained optimization:

$$\begin{aligned} &\text{maximize } \text{ELBO}, \\ &\text{s.t. } (13). \end{aligned} \quad (14)$$

By the lagrangian multiplier method, we have the new loss function:

$$\mathcal{L} = -\text{ELBO} + \alpha \mathbf{H}(\mathbf{A}) \quad (15)$$

where  $\alpha$  denotes the regularization hyperparameter.

## 3 EXPERIMENTS

In this section, we present the extensive experiments conducted on one semi-simulated dataset and five real-world datasets to demonstrate the effectiveness of the proposed CSC, with an emphasis on answering the following research questions:

- Can CSC obtain a useful causal graph of confounders without relevant labels?
- Can CSC achieve better performance compared to other baselines?
- How do the causal relationships of confounders enhance the model's performance?
- How do the number of confounders and the hyperparameter  $\alpha$  influence the performance of CSC?

### 3.1 Dataset

It is difficult to verify the effectiveness of the causal graphs learned by CSC as the information of confounders is unobserved in the real dataset. Thus, we first validate the effectiveness of causal graphs on synthetic datasets and subsequently evaluate the recommendation performance of CSC on real-world datasets.

**3.1.1 Synthetic Dataset.** We conduct experiments on synthetic data, generated by the following process: We first assume that users are influenced by four confounders, where the exogenous variables for each confounder are generated by sampling from Gaussian distributions with mean and variance sampled from uniform distributions  $[-3, 3]$  and  $[0.01, 4]$ , respectively. The intrinsic preferences of users are sampled from a standard normal distribution. Given the user’s preference value  $\mathcal{U}$ , we obtain the user’s personalized weights  $w$  by sampling from a Poisson distribution. We generate samples using the causal structure model as shown in Eq 2. Finally, we input the confounders and user preferences into a two-layer MLP to generate the final observed value  $\mathcal{X}$ . Additional details and a formal description can be found in the Appendix A.4.

**3.1.2 Real-World datasets.** To comprehensively and fairly validate the effectiveness of the model, we conducted experiments using five publicly available datasets that encompass a variety of recommendation scenarios (such as movies and clothes) and different densities. We select three datasets of varying sizes ranging from 100k to 20M: ML-100K, ML-1M, and ML-20M collected from the MovieLens website<sup>3</sup> to validate the robustness of the model to the dataset size. Additionally, we leverage the Yelp dataset, a rich source of reviews, businesses, users, tips, and check-in data<sup>4</sup>, to validate the impact of the model on different sparsity levels. In addition, we utilized the TaFeng dataset<sup>5</sup>, which consists of Chinese grocery store transaction data from November 2000 to February 2001, to conduct ‘do-operation’ experiments. This dataset was chosen due to its inclusion of price information regarding items purchased by users. Following prior works [1, 13], we split the dataset into 70% for training, 20% for testing, and the remaining for validation. All user ratings greater than or equal to four are set to 1, while the rest are set to 0.

**3.1.3 Baselines.** We compare our method with the corresponding base models and the state-of-the-art de-confounding methods that can alleviate the confounding bias in recommender systems in the presence of unobserved confounders. **Multi-VAE** [5]: Variational autoencoders (VAEs) to collaborative filtering for implicit feedback with VAE. **Muti-DAE** [5]: variational autoencoders (VAEs) to collaborative filtering for implicit feedback with DAE. **Macrid-VAE** [15]: Achieves macro disentanglement by inferring the high-level concepts associated with user intentions while simultaneously capturing a user’s preference regarding the different concepts. **Rec-VAE** [11]: RecVAE introduces several novel ideas to improve Multi-VAE. **CDAE** [17]: A novel method for top-N recommendation that utilizes the idea of Denoising Auto-Encoders. **InvPref** [16]: InvPref assumes the existence of multiple environments as proxies of unmeasured confounders and applies invariant learning to learn the user’s invariant preference. **IDCF** [22]: A general de-confounded recommendation framework that applies proximal causal inference to infer the unmeasured confounders and identify the counterfactual feedback with theoretical guarantees.

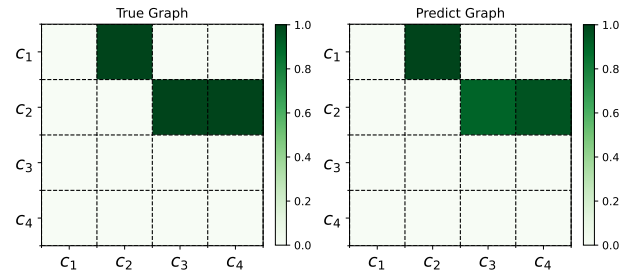


**Figure 6: In the graph prediction experiment on the synthetic data, true graph (left), and the predicted graph (right).**

## 3.2 Experimental Settings

**3.2.1 Setups.** We implement CSC and baselines in PyTorch. All models are trained with the Adam optimizer via early stopping at patience = 10. We set the learning rate to  $1e-3$  and the  $l_2$ -regularization weight to  $1e-6$ . For CSC, we tune the hyper-parameter  $\alpha$  in the range of  $[0, 10, 50, 100]$  and concepts  $k$  in the range of  $[1, 2, 4, 8]$  for different data sets. To detect significant differences in CSC and the best baseline on each data set, we repeated their experiments five times by varying the random seeds. We choose the average performance to report. All ranking metrics are computed at a cutoff  $K = [10, 30]$  for the Top- $k$  recommendation. Our implementation of the baselines is based on the original paper or the open codebase Recbole [24].

**3.2.2 Evaluation Metrics.** Note that the sampling-based evaluation approach does not truly reflect the ability of the model to capture the true preferences of users, simply fitting the data may also have better performance. To this end, we report the all-ranking performance w.r.t. two widely used metrics: Recall and NDCG cut at  $K = [10, 30]$ . To measure the price of recommended items, we use average price rank (AVP) as the other indicator, and the formula is:

$$\text{AveragePopularity(AVP)}@K = \frac{1}{|U|} \sum_{u \in U} \frac{\sum_{i \in \text{Price}_u} \phi(i)}{|\text{Price}_u|}$$

## 3.3 Performance on the Synthetic Dataset (RQ1).

The synthetic data set we used contained four confounders, resulting in a power of  $3^4$  possible relationships. Although the number of categories is not extensive, it still poses a challenging task. By the causal relationships between confounders present in the synthetic data, we can unambiguously determine the ability of CSC to capture the causal relationships between confounders. Due to the strong correlation between the local graph and users, we only present here the global graph obtained by the CSC. As shown in Figure 6, the global graph learned by CSC is well aligned with the ground truth graph, thus demonstrating the ability of CSC to capture the causal relationships between confounders effectively. It is important to emphasize that we used the *Gumbel-Sigmoid* shown in Eq. 4, resulting in an approximation of a binary causal graph by CSC. The final experimental results strongly support this approach.

<sup>3</sup><https://grouplens.org/datasets/movielens/>

<sup>4</sup><https://www.kaggle.com/datasets/yelp-dataset/yelp-dataset>

<sup>5</sup><https://www.kaggle.com/datasets/chiranjivdas09/ta-feng-grocery-dataset>

Datasets	Metric	k	Multi-VAE	Multi-DAE	Macrid-VAE	Rec-VAE	CDAE	InvPref	ICDF	CSC	Imp.
ML-100K	Recall	10	0.0971	0.0986	0.0970	<u>0.1031</u>	0.0066	0.0873	0.0727	<b>0.1185</b>	14.94%
		30	0.2377	0.2219	0.2353	<u>0.2442</u>	0.0173	0.2470	0.1687	<b>0.2677</b>	9.21%
	NDCG	10	0.1221	0.1121	0.1298	<u>0.1324</u>	0.0069	0.1217	0.0930	<b>0.1350</b>	1.96%
		30	0.1531	0.1398	0.1623	<u>0.1654</u>	0.0110	0.1627	0.1219	<b>0.1790</b>	8.22%
ML-1M	Recall	10	0.0590	0.0597	0.0589	<u>0.0611</u>	0.0454	0.0595	0.0480	<b>0.0673</b>	10.14%
		30	0.1561	0.1581	0.1566	<u>0.1602</u>	0.1141	0.0154	0.1199	<b>0.1664</b>	3.87%
	NDCG	10	0.0892	0.0878	0.0907	<u>0.0925</u>	0.0825	0.0896	0.0778	<b>0.0955</b>	3.24%
		30	0.1159	0.1154	0.1171	<u>0.1192</u>	0.0968	0.1155	0.1021	<b>0.1241</b>	4.11%
ML-20M	Recall	10	0.0884	0.0870	0.0859	<u>0.0907</u>	0.906	0.0537	0.0586	<b>0.0952</b>	4.96%
		30	0.2140	0.2180	0.2100	0.2155	<u>0.2181</u>	0.1303	0.1247	<b>0.2233</b>	2.38%
	NDCG	10	0.0985	0.0978	<u>0.0990</u>	0.0954	0.0957	0.0698	0.0717	<b>0.1081</b>	9.19%
		30	<u>0.1399</u>	0.1389	0.1366	0.1360	0.1338	0.0920	0.0903	<b>0.1471</b>	5.15%
TaFeng	Recall	10	0.0381	0.0371	0.0358	0.0322	<u>0.0397</u>	0.0376	0.0315	<b>0.0456</b>	14.86%
		30	0.0795	0.0789	0.0789	<u>0.0798</u>	0.0711	0.0793	0.0748	<b>0.0849</b>	6.39%
	NDCG	10	0.0340	0.0381	0.0401	<u>0.0404</u>	0.0361	0.0336	0.0370	<b>0.0446</b>	10.39%
		30	0.0480	0.0471	<u>0.0538</u>	0.0440	0.0450	0.0476	0.0464	<b>0.0559</b>	3.91%
Yelp	Recall	10	0.0255	0.0249	<u>0.0266</u>	0.0252	0.0092	0.0196	0.0167	<b>0.0292</b>	9.77%
		30	0.0578	0.0568	0.0537	<u>0.0591</u>	0.0196	0.0434	0.0489	<b>0.0642</b>	8.63%
	NDCG	10	0.0161	0.0158	<u>0.0178</u>	0.0170	0.0063	0.0124	0.0133	<b>0.0205</b>	15.16%
		30	0.0224	0.0219	<u>0.0259</u>	0.0235	0.0093	0.0197	0.0201	<b>0.0312</b>	20.46%

**Table 2: Overall performance of applying our model on five real-world datasets. The best result in each column is in bold; The best baseline result in each line is underlined. The recommendation performance is evaluated as a ranking task. Higher Recall and NDCG mean better model performance.**

### 3.4 Comparison with Baselines (RQ2)

The comparison between CSC and various baselines is shown in Table 2. The best results (compared across four classes) are shown in bold, and the runner-ups are underlined. In summary, we have the following observations: (1) The table demonstrates that the CSC model consistently outperforms the baselines regarding Recall and NDCG across various datasets and evaluation metrics. Specifically, CSC achieves the highest Recall and NDCG scores in nearly all cases, indicating its superior ability to recommend relevant items to users. Remarkably, CSC substantially improves Recall and NDCG compared to the baselines, often ranging from 2% to nearly 15% across different datasets and evaluation settings. (2) The datasets with higher sparsity levels, such as ML-20M, Yelp, and TaFeng, often present more challenges for traditional recommender systems due to the scarcity of user-item interactions. However, the CSC model demonstrates substantial improvements in these datasets, suggesting its robustness in handling sparse data and providing meaningful recommendations despite the challenges posed by data sparsity. (3) The de-confounding methods ICDF and Invpref exhibit weaker recommendation performance compared to VAE-based approaches, primarily because VAEs more accurately model user preferences in the latent space. Thus, using latent space by CSC to separate confounders leads to improved performance. In summary, the comprehensive analysis of the performance of CSC across these datasets underscores its potential to significantly enhance recommendation quality and user engagement across a spectrum of real-world applications. The consistent outperformance over baseline models highlights the efficacy of integrating causal graph-based approaches in recommender systems, addressing unobserved confounders and providing more accurate and satisfying recommendations.

Datasets	$CSC^{non}$	$CSC^g$	$CSC^l$	$CSC^{g+l}$
ML-20M	0.1012	0.1038 (+2.25%)	0.1037 (+2.47%)	0.1049 (+3.66%)
Yelp	0.0130	0.0138 (+6.15%)	0.0136 (+4.62%)	0.0143 (+10.00%)

**Table 3: Ablation experiments on global and local graphs conducted on ML-20M and Yelp with NDCG@1.  $CSC^{non}$ : removing both global and local graphs,  $CSC^g$ : removing local graph,  $CSC^l$ : removing global graph,  $CSC^{g+l}$ : deploying both global and local graphs simultaneously. (+xx%): percentage of improvement on NDCG of  $CSC^g$ ,  $CSC^l$ ,  $CSC^{g+l}$  over  $CSC^{non}$ .**

### 3.5 Ablation Study (RQ3).

**3.5.1 Effectiveness of Global and Local Graphs.** The table 3 presents results for different variants involving both the global and local graphs:  $CSC^g$  (without local graph),  $CSC^l$  (without global graph), and  $CSC^{g+l}$  (with both global and local graphs). We have the following observations: (1) Using either the global graph or the local graph alone results in improved performance on the dataset. The global graph captures the macro-level causal relationships among confounders, albeit losing specificity to users. On the other hand, the local graph captures user specificity but loses the accurate relationships between confounders. Both contribute partially to the causal relationships between confounders, leading to an enhancement in model performance. (2) Simultaneously using the local and global graphs results in a performance improvement greater than the sum of their individual contributions. The global graph can correct the erroneous causal relationships between confounders in the local graph, while the local graph assigns user-specific weights to the global graph. The synergy of both significantly enhances

Metric	$c_1$	$c_2$	$c_3$	$c_4$	CSC
AVP@10	14.9712	13.9709	13.9710	13.9710	13.9709

**Table 4: "do-operation" experiments conducted on the Tafeng dataset with the number of confounders,  $K = 4$ .**

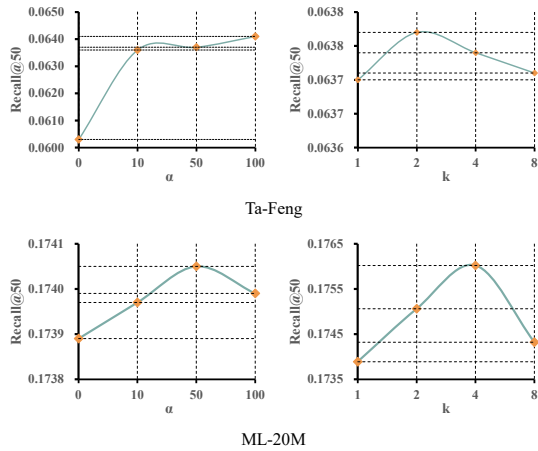


**Figure 7: Sensitivity of CSC with different values of  $\alpha$  and  $K$  on TaFeng and ML-20M dataset.**

the model’s performance. In summary, the collaborative effect of both graphs significantly enhances recommendation quality by enabling a more comprehensive understanding of user behavior and preferences, creating a powerful model for accurate and effective recommendations.

**3.5.2 "do-operation" with Mask Graph.** We conducted common 'do-operation' experiments in the causal inference domain on the TaFeng dataset, and the results are shown in Table 4. We employed four concepts of confounders ( $k = 4$ ) to model the unobserved confounders in the dataset. We used the prices of items recommended to the users to determine the effect of the confounders. It is important to note that applying the 'do-operation' to a confounder  $c_i$  involves using an additional masking matrix and performing a dot product with the global graph. In the masking matrix, the  $i$ -th row is all zeros (indicating no influence as a parent node), and the rest of the rows are all ones. From the table, we can observe that when performing the 'do-operation' on  $c_2$ ,  $c_3$ , and  $c_4$ , the average prices of recommended items do not significantly differ from CSC. This implies that these three confounders do not influence the decisions of users based on item prices. However, when we perform the 'do-operation' on  $c_1$ , there is a noticeable increase in the average price of recommended items, indicating that  $c_1$  captures the sensitivity of users to item prices. Furthermore, the results of the 'do-operation' experiments also demonstrate that the CSC model can capture the influence of confounders, providing evidence of the effectiveness of the modeling described in Eq. 2.

### 3.6 Sensitivity Analysis (RQ4).

#### 3.6.1 Directed Acyclic Graph Constraint Hyperparameter $\alpha$ .

We used various values of  $\alpha$  on the ML-20M and TaFeng datasets to verify the influence of the strength of the directed acyclic graph (DAG) constraint. Figure 7 (left side) shows that a larger  $\alpha$  implies a stronger constraint. Consequently, as the  $\alpha$  value increases, we obtain a more compliant graph, improving model performance. However, an excessively large  $\alpha$  reduces edges in the learned graph to meet the stringent constraint, thus causing a decrease in model performance.

#### 3.6.2 The Concept Number $K$ .

We used various values of  $K$  on the ML-20M and TaFeng datasets to verify the influence of the number of confounders. Figure 7 (right side) shows that a larger  $K$  implies a more diverse set of confounders. Consequently, as  $K$  increases, we obtain a finer-grained representation of the confounders, improving model performance. However, an excessively large  $K$  can cause the learned representation of confounders to be more than the actual number of concepts influencing the data, leading to model overfitting and a subsequent decrease in performance.

## 4 RELATED WORK

### 4.1 Causal Structure Learning

We refer to causal representations constructed by causal graphs as causal representations. Over the past few decades, discovering causal graphs from purely observational data has garnered significant attention. [25] proposed NOTEARs with a fully differentiable DAG constraint for causal structure learning, [12] show the identifiability of learned causal structure from interventional data. The community has raised interest in combining causality and disentangled representation and [3] proposed a method called CausalGAN, which supports "do-operation" on images but it requires the causal graph given as a prior. In this work, we drew on related ideas, improved upon them successfully, and applied them to recommender systems.

### 4.2 Deconfound in Recommendation

With the increasing popularity of causal inference as a method to mitigate bias in recommender systems, researchers are paying more attention to the challenges posed by confounding biases. Confounding bias is prevalent in recommender systems due to various confounders. While some studies have addressed specific confounding biases, such as item popularity [14, 23], many unobservable confounders may also exist. The mainstream approaches can be broadly categorized into two types: (1) [19, 26] utilize additional signals as instrumental or proxy variables to mitigate confounding bias. (2) [18, 27] consider a multiple-treatment setting and infer surrogate confounders from user exposure, incorporating them into the preference prediction model. However, they did not address the challenge of confounders in the absence of labels.

## 5 CONCLUSION

Predicting user preferences in the presence of confounders is a challenging problem. We first redefined the problem, incorporating the influence of confounders into the model. We proposed a mild assumption to separate user preferences from confounders



and used a combination of local and global graphs to capture the causal relationships between confounders and user specificity. Finally, we proposed a VAE-based model called CSC. Extensive experiments are conducted on a synthetic dataset and five real-world datasets to demonstrate the model's superiority. We theoretically proved the model's Evidence Lower Bound (ELBO) and the learned graph's identifiability. Furthermore, we employed the 'do-operation' method to validate the controllability of the model, potentially offering users fine-grained control over the objectives of their recommendation lists with the learned causal graphs. Future work can explore advanced unsupervised clustering methods to obtain categories of confounders further, addressing the limitation of uncertainty in the impact categories of obtained confounders on user preferences.

## REFERENCES

- [1] Yiheng Jiang, Yuanbo Xu, Yongjian Yang, Funing Yang, Pengyang Wang, and Hui Xiong. 2023. TriMLP: Revenge of a MLP-like Architecture in Sequential Recommendation. arXiv:2305.14675 [cs.LG]
- [2] Diederik P Kingma and Max Welling. 2013. Auto-Encoding Variational Bayes. In *International Conference on Learning Representations*.
- [3] Murat Kocaoglu, Christopher Snyder, Alexandros G. Dimakis, and Sriram Vishwanath. 2017. CausalGAN: Learning Causal Implicit Generative Models with Adversarial Training. arXiv:1709.02023 [cs.LG]
- [4] Sébastien Lachapelle, Philippe Brouillard, Tristan Deleu, and Simon Lacoste-Julien. 2019. Gradient-Based Neural DAG Learning. *CoRR* abs/1906.02226 (2019). arXiv:1906.02226 <http://arxiv.org/abs/1906.02226>
- [5] Dawen Liang, Rahul G. Krishnan, Matthew D. Hoffman, and Tony Jebara. 2018. Variational Autoencoders for Collaborative Filtering. arXiv:1802.05814 [stat.ML]
- [6] Francesco Locatello, Stefan Bauer, Mario Lucic, Gunnar Raetsch, Sylvain Gelly, Bernhard Schölkopf, and Olivier Bachem. 2019. Challenging Common Assumptions in the Unsupervised Learning of Disentangled Representations. In *Proceedings of the 36th International Conference on Machine Learning (Proceedings of Machine Learning Research, Vol. 97)*, Kamalika Chaudhuri and Ruslan Salakhutdinov (Eds.), PMLR, 4114–4124. <https://proceedings.mlr.press/v97/locatello19a.html>
- [7] Christopher Maddison, Andriy Mnih, and Yee Teh. 2017. The Concrete Distribution: A Continuous Relaxation of Discrete Random Variables.
- [8] Ignavier Ng, Shengyu Zhu, Zhuangyan Fang, Haoyang Li, Zhitang Chen, and Jun Wang. [n.d.]. *Masked Gradient-Based Causal Structure Learning*. 424–432. <https://doi.org/10.1137/1.9781611977172.48> arXiv:<https://pubs.siam.org/doi/pdf/10.1137/1.9781611977172.48>
- [9] Jonas Peters, Joris M. Mooij, Dominik Janzing, and Bernhard Schölkopf. 2014. Causal Discovery with Continuous Additive Noise Models. *Journal of Machine Learning Research* 15, 58 (2014), 2009–2053. <http://jmlr.org/papers/v15/peters14a.html>
- [10] Xinwei Shen, Furui Liu, Hanze Dong, Qing Lian, Zhitang Chen, and Tong Zhang. 2022. Weakly Supervised Disentangled Generative Causal Representation Learning. *Journal of Machine Learning Research* 23, 241 (2022), 1–55. <http://jmlr.org/papers/v23/21-0080.html>
- [11] Ilya Shenbin, Anton Alekseev, Elena Tutubalina, Valentin Malykh, and Sergey I Nikolenko. 2020. Recvae: A new variational autoencoder for top-n recommendations with implicit feedback. In *Proceedings of the 13th international conference on web search and data mining*. 528–536.
- [12] Robert Tillman and Peter Spirtes. 2011. Learning equivalence classes of acyclic models with latent and selection variables from multiple datasets with overlapping variables. In *Proceedings of the Fourteenth International Conference on Artificial Intelligence and Statistics (Proceedings of Machine Learning Research, Vol. 15)*, Geoffrey Gordon, David Dunson, and Miroslav Dudik (Eds.), PMLR, Fort Lauderdale, FL, USA, 3–15. <https://proceedings.mlr.press/v15/tillman11a.html>
- [13] En Wang, Yiheng Jiang, Yuanbo Xu, Liang Wang, and Yongjian Yang. 2022. Spatial-temporal interval aware sequential POI recommendation. In *2022 IEEE 38th International Conference on Data Engineering (ICDE)*. IEEE, 2086–2098.
- [14] Wenjie Wang, Fuli Feng, Xiangnan He, Xiang Wang, and Tat-Seng Chua. 2021. Deconfounded Recommendation for Alleviating Bias Amplification (*KDD '21*). Association for Computing Machinery, New York, NY, USA, 1717–1725. <https://doi.org/10.1145/3447548.3467249>
- [15] Xin Wang, Hong Chen, Yuwei Zhou, Jianxin Ma, and Wenwu Zhu. 2023. Disentangled Representation Learning for Recommendation. *IEEE Transactions on Pattern Analysis and Machine Intelligence* 45, 1 (2023), 408–424. <https://doi.org/10.1109/TPAMI.2022.3153112>
- [16] Zimu Wang, Yue He, Jiashuo Liu, Wenchao Zou, Philip S Yu, and Peng Cui. 2022. Invariant preference learning for general debiasing in recommendation. In *Proceedings of the 28th ACM SIGKDD Conference on Knowledge Discovery and Data Mining*, 1969–1978.
- [17] Yao Wu, Christopher DuBois, Alice X Zheng, and Martin Ester. 2016. Collaborative denoising auto-encoders for top-n recommender systems. In *Proceedings of the ninth ACM international conference on web search and data mining*. 153–162.
- [18] Shuyuan Xu, Jianchao Ji, Yunqi Li, Yingqiang Ge, Juntao Tan, and Yongfeng Zhang. 2023. Causal Inference for Recommendation: Foundations, Methods and Applications. arXiv:2301.04016 [cs.IR]
- [19] Shuyuan Xu, Juntao Tan, Shelby Heinecke, Vena Jia Li, and Yongfeng Zhang. 2023. Deconfounded Causal Collaborative Filtering. *ACM Transactions on Recommender Systems* 1, 4 (oct 2023), 1–25. <https://doi.org/10.1145/3606035>
- [20] Mengyue Yang, Furui Liu, Zhitang Chen, Xinwei Shen, Jianye Hao, and Jun Wang. 2021. CausalVAE: Disentangled Representation Learning via Neural Structural Causal Models. In *Proceedings of the IEEE/CVF Conference on Computer Vision and Pattern Recognition (CVPR)*. 9593–9602.
- [21] Yue Yu, Jie Chen, Tian Gao, and Mo Yu. 2019. DAG-GNN: DAG Structure Learning with Graph Neural Networks. In *Proceedings of the 36th International Conference on Machine Learning (Proceedings of Machine Learning Research, Vol. 97)*, Kamalika Chaudhuri and Ruslan Salakhutdinov (Eds.), PMLR, 7154–7163. <https://proceedings.mlr.press/v97/yyu19a.html>
- [22] Qing Zhang, Xiaoying Zhang, Yang Liu, Hongning Wang, Min Gao, Jiheng Zhang, and Ruocheng Guo. 2023. Debiasing Recommendation by Learning Identifiable Latent Confounders. *arXiv preprint arXiv:2302.05052* (2023).
- [23] Yang Zhang, Fuli Feng, Xiangnan He, Tianxin Wei, Chonggang Song, Guohui Ling, and Yongdong Zhang. 2021. Causal Intervention for Leveraging Popularity Bias in Recommendation (*SIGIR '21*). Association for Computing Machinery, New York, NY, USA, 11–20. <https://doi.org/10.1145/3404835.3462875>
- [24] Wayne Xin Zhao, Yupeng Hou, Xingyu Pan, Chen Yang, Zeyu Zhang, Zihan Lin, Jingsen Zhang, Shuqing Bian, Jiakai Tang, Wenqi Sun, et al. 2022. RecBole 2.0: Towards a More Up-to-Date Recommendation Library. In *Proceedings of the 31st ACM International Conference on Information & Knowledge Management*. 4722–4726.
- [25] Xun Zheng, Bryon Aragam, Pradeep Ravikumar, and Eric P. Xing. 2018. DAGs with NO TEARS: Continuous Optimization for Structure Learning. arXiv:1803.01422 [stat.ML]
- [26] Xinyuan Zhu, Yang Zhang, Fuli Feng, Xun Yang, Dingxian Wang, and Xiangnan He. 2022. Mitigating Hidden Confounding Effects for Causal Recommendation. *ArXiv* abs/2205.07499 (2022). <https://api.semanticscholar.org/CorpusID:248811475>
- [27] Yaochen Zhu, Jing Yi, Jiayi Xie, and Zhenzhong Chen. 2022. Deep Causal Reasoning for Recommendations. <https://api.semanticscholar.org/CorpusID:245769824>

## A PROOFS

### A.1 Proof of Lemma 1

PROOF. First, let's consider the case where the  $g_i(\cdot)$  is a constant, w.r.t.  $c_j$  whether the  $A_{ji} = 0$  or  $1$  do not affect  $c_i$ , but will change the causal graph  $\mathcal{H}$ , so when  $g_i(\cdot)$  is constant, we can not uniquely identified the  $\mathcal{H}$  from  $P(\mathbf{C})$ . Fortunately, in recommender systems,  $g_i(\cdot)$  usually satisfies the non-constant condition. Then, we restrict  $g_i$  to be non-constant, w.r.t. all  $c_j$ ,  $j \neq i$  to meet the causal minimality condition.

It suffices to show that if  $c_j$  is not a parent of  $c_i$  in  $\mathcal{H}$ , then  $c_j$  is not a parent of  $c_i$  in  $\mathcal{G}$ , either. That  $c_j$  is not a parent of  $c_i$  in  $\mathcal{H}$  indicates  $A_{ji} = 0$ . Therefore,  $g_i(A_i \odot \mathbf{C})$  is a constant function w.r.t.  $c_j$ . For the reduced SEM with functions  $g_i$ 's and causal DAG  $\mathcal{G}$ , we conclude that  $c_j \notin \text{cpa}_i$  and the input arguments of  $g_i$  do not contain. Thus,  $c_j$  cannot be a parent of  $c_i$  in  $\mathcal{G}$ .  $\square$

### A.2 Proof of proposition 1

PROOF. Recall that the reduced SEM with  $g_i$ 's and graph  $\mathcal{G}$  satisfies the causal minimality condition and has the same distribution  $P(\mathbf{C})$ . With the identifiability result of restricted ANMs [9], we know that  $\mathcal{G}$  is identical. Applying Lemma 1 completes the proof.  $\square$

### A.3 Proof of Evidence Lower Bound

$$\ln p_\theta(x_u) \geq E_{p_\theta(\mathbf{C})} \{ E_{q_\theta(z_u|x_u, \mathbf{C})} [\ln p_\theta(x_u|z_u, \mathbf{C})] - D_{KL}(q_\theta(z_u|x_u, \mathbf{C}) \| p_\theta(z_u)) \} .$$

PROOF. Note that:

$$\begin{aligned} q_\theta(z_u, \mathbf{C}|x_u) &= q_\theta(z_u|x_u, \mathbf{C})p_\theta(\mathbf{C}), \\ D_{KL}(q_\theta(z_u, \mathbf{C}|x_u) \| p_\theta(z_u, \mathbf{C})) \\ &= D_{KL}(q_\theta(z_u|x_u, \mathbf{C})p_\theta(\mathbf{C}) \| p_\theta(z_u)p_\theta(\mathbf{C})) \\ &= E_{p_\theta(\mathbf{C})} [D_{KL}(q_\theta(z_u|x_u, \mathbf{C}) \| p_\theta(z_u))] . \end{aligned}$$

$$\begin{aligned} \ln p_\theta(x_u) &= E_{q_\theta(z_u, \mathbf{C}|x_u)} [\ln p_\theta(x_u)] \\ &= E_{q_\theta(z_u, \mathbf{C}|x_u)} \left[ \ln \frac{p_\theta(x_u, z_u, \mathbf{C})}{p_\theta(z_u, \mathbf{C}|x_u)} \right] \\ &= E_{q_\theta(z_u, \mathbf{C}|x_u)} \left[ \ln \frac{q_\theta(z_u, \mathbf{C}|x_u)}{p_\theta(z_u, \mathbf{C}|x_u)} \right] + E_{q_\theta(z_u, \mathbf{C}|x_u)} \left[ \ln \frac{p_\theta(x_u, z_u, \mathbf{C})}{q_\theta(z_u, \mathbf{C}|x_u)} \right] \\ &= E_{q_\theta(z_u, \mathbf{C}|x_u)} \left[ \ln \frac{q_\theta(x_u, z_u, \mathbf{C})}{p_\theta(z_u, \mathbf{C}|x_u)} \right] + E_{q_\theta(z_u, \mathbf{C}|x_u)} [\ln p_\theta(x_u|z_u, \mathbf{C})] \\ &\quad + E_{q_\theta(z_u, \mathbf{C}|x_u)} \left[ \ln \frac{p_\theta(z_u, \mathbf{C})}{p_\theta(z_u, \mathbf{C}|x_u)} \right] \\ &= D_{KL}(q_\theta(z_u, \mathbf{C}|x_u) \| p_\theta(z_u, \mathbf{C}|x_u)) + E_{q_\theta(z_u, \mathbf{C}|x_u)} [\ln p_\theta(x_u|z_u, \mathbf{C})] \\ &\quad - D_{KL}(q_\theta(z_u, \mathbf{C}|x_u) \| p_\theta(z_u, \mathbf{C})) \\ &\geq E_{q_\theta(z_u, \mathbf{C}|x_u)} [\ln p_\theta(x_u|z_u, \mathbf{C})] - D_{KL}(q_\theta(z_u, \mathbf{C}|x_u) \| p_\theta(z_u, \mathbf{C})) \\ &= E_{p_\theta(\mathbf{C})} \{ E_{q_\theta(z_u|x_u, \mathbf{C})} [\ln p_\theta(x_u|z_u, \mathbf{C})] \\ &\quad - D_{KL}(q_\theta(z_u|x_u, \mathbf{C}) \| p_\theta(z_u)) \} . \end{aligned}$$

□

### A.4 Synthetic Dataset Details.

For synthetic data experiments, the number of user samples is 300, and for each user sample 500 items. We assume that users are influenced by four different categories of confounders and the causal relationships of these four confounders can be generated using Eq 2. Specifically, we consider the following causal structural model:

$$\begin{aligned} n_1 &= \mathcal{N}(\lambda_1, \beta_1), \\ n_2 &= \mathcal{N}(\lambda_2, \beta_2), \\ n_3 &= \mathcal{N}(\lambda_3, \beta_3), \\ n_4 &= \mathcal{N}(\lambda_4, \beta_4), \\ c_1 &= n_1, \\ c_2 &= w_2(u)(c_1) + n_2, \\ c_3 &= w_3(u)(c_2) + n_3, \\ c_4 &= w_4(u)(c_2) + n_4. \end{aligned} \tag{16}$$

where  $\lambda_i$  and  $\beta_i$  are the mean and variance of the Gaussian distribution, we sample the  $\lambda_i$  and  $\beta_i$  from the uniform distribution  $[-3, 3]$  and  $[0.01, 4]$ , respectively. We sample the user-specific weight  $w_i$  from Poisson distribution with the give  $u$ :

$$u = \mathcal{N}(0, 1). \tag{17}$$

Finally, given the set of confounders and users, we can generate the final observed value  $\mathcal{X}$  through a non-linear function  $g(\cdot)$ :

$$\mathcal{X} = g(c_1, c_2, c_3, c_4, u). \tag{18}$$

In our experiments, we used a two-layer MLP for the blending generation.